Ceramics-Silikáty 67 (1), 1-9 (2023)
www.ceramics-silikaty.cz doi: 10.13168/cs.2022.0054

ACTIVATION OF METAKAOLIN BY CaO AND $CaSO_4$ ANHYDRITE II

FRANTIŠEK ŠKVÁRA*, #MARTINA ŠÍDLOVÁ*, ROSTISLAV ŠULC**, KLÁRA PULCOVÁ*

*Department of Glass and Ceramics, Faculty of Chemical Technology, University of Chemistry and Technology Prague, Technická 5, 166 28 Prague, Czech Republic
**Department of Building Technology, Faculty of Civil Engineering, Czech Technical University in Prague, Jugoslávských partyzánů 1580/3, 160 00 Prague, Czech Republic

#E-mail: martina.sidlova@vscht.cz

Submitted October 7, 2022; accepted December 7, 2022

Keywords: Metakaolin, Lime activation, Hydraulic binder, Roman cement, $CaSO_4$ anhydrite II

The paper presented deals with the activation of metakaolin enabling the preparation of a new hydraulic binder. Activation of metakaolin is carried out using calcium oxide or hydroxide and gypsum or $CaSO_4$ in the form of anhydrite II. CaO and $CaSO_4$ anhydrite II were found to be more effective activators of metakaolin compared to $Ca(OH)_2$ and $CaSO_4 \cdot 2H_2O$. The binding phase is represented here by an amorphous C–A–S–H phase accompanied with a C–S–H phase indicating similarity with Roman cement. Several crystalline hydrating products are present in the binder with ettringite being the major phase, and $CaCO_3$, $Ca(OH)_2$ and $CaSO_4 \cdot 2H_2O$ constituting its minor phases. In its composition, the binder, which is prepared synthetically, agrees with that of hydrated FBC ashes, and was found to be stable over a period of 2.8 years achieving strengths comparable to those of Portland cement.

INTRODUCTION

In recent years, the world-wide effort to reduce CO_2 has led the society to search for new substitutes of Portland cement (PC). Greater replacement of cement with supplementary cementitious materials (SCMs) in PC is one of the most realistic strategies to lower the environmental impact. Besides commonly used materials such as fly ash (FA) and blast furnace slag, calcined clays are gaining greater importance [1] as they can exhibit pozzolanic properties [2]. R. Snellings states that in 2016 the use of calcined clays as SCMs reached 2-3 Mt compared to blast furnace slag with 300-360 Mt or FA (rich in Si and Ca) with 700-1100 Mt. The data on the use of calcined clays used as an additive in PC are detailed in publications [3-7]. A new type of a hydraulic composite binder presented is created by the combination of calcined clay, limestone and PC (FutureCem, LC^3 cement) [8, 9]. Also, calcined clays can be used to hydrate fluidized bed combustion (FBC) ashes [10-13]. FBC ashes contain not only calcined clay, but also quick lime and insoluble $CaSO_4$ anhydrite AII [14]. However, the hydration of FBC ashes is rather complicated due to their volume instability [12] caused by the occurrence of ettringite. Nevertheless, a number of experiments showed that it was possible to eliminate volume expansion and to reach stable firmness lasting for years by grinding and mixing FBC ash and adding polycarboxylates to tap water [15]. Furthermore, it was found that the hardened binder contained not just a C–S–H phase (Calcium Silicate Hydrate), but also a C–A–S–H phase (Calcium Aluminum Silicate Hydrate). The latter was actually identified in medieval buildings and is deemed to be responsible for their long-lasting stability.

In general, clays and other aluminosilicates in their original crystalline forms cannot be practically activated by the addition of lime activators. Only the amorphous form after calcination allows their activation. Natural aluminosilicate crystalline substances such as kaolin contain water molecules in their structure. Calcination to temperatures above 500 °C leads to dehydration and the formation of an amorphous substance – metakaolin, as shown in Equation 1

$$Al_2O_3 \cdot 2SiO_2 \cdot 2H_2O \rightarrow Al_2O_3 \cdot 2SiO_2 + 2H_2O \qquad (1)$$

When heated above 925 °C, a crystalline spinel and amorphous SiO_2 are formed. Natural calcined aluminosilicate compounds displaying amorphous characteristics also contain crystalline substances, especially quartz. In nature, several amorphous aluminosilicate substances can be found, such as pozzolans, volcanic dust, etc. These substances do not have water molecules in their structure, thus allowing lime activation [16].

The principle of lime activation was described in the work “10 books on architecture” [17] and was applied in Roman buildings. The results of material research on Roman concrete from recent years were published in the book “Building for Eternity” [18]. Roman cement consisted of a mixture of lime and crushed volcanic materials or bricks fired at lower temperatures than those used at present. Typically, compressive strength of Ro-

man concrete reached 5-15 MPa. The construction activity of the Romans using Roman cement was terminated by the invasion of barbarians in the years 410-455 AD and the following demise of the Roman Empire. The hydraulic binders made of lime with pozzolan, known in ancient Rome, were also known to Central American pre-Columbian civilizations such as the Mayans [19-21]. In contrast, the Middle Ages saw hydraulic lime being used as a binder. Hydraulic lime was produced by burning impure limestone containing Si and Al components primarily in the form of clay minerals. This type of hydraulic lime manifested medium to strong hydraulic properties. Its burning temperature was 800-1200 °C, i.e. below the temperature of sintering. These hydraulic lime binders are known as Romanesque cement and represent the transition between hydraulic lime and PC.

Today, the lime activation by means of $Ca(OH)_2$ is successfully applied to ash and slag mixtures [22], or sulfate activation employing $CaSO_4$ with Na_2SO_4 may also be used. The sulfate-lime activation of alumino-silicate substances is known for mixed activators such as CaO and $CaSO_4 \cdot 2H_2O$ [23] or $Ca(OH)_2$ and $CaSO_4 \cdot 1/2H_2O$ [24]. In addition, the sulfate-lime activation of aluminosilicate substances was studied in the systems of $Ca(OH)_2$ and $CaSO_4 \cdot 2H_2O$ [25], $Ca(OH)_2$ and $CaSO_4$ anhydrite III (low-temperature, soluble an-hydrite) [26], or $CaSO_4 \cdot 2H_2O$ and Na_2CO_3. Moreover, there is also an option of calcium sulfate activation of clays in FBC ashes that contain a mixture of clay, $CaSO_4$ anhydrite II and CaO as described earlier.

Besides lime activation, it is possible to activate amorphous aluminosilicates such as metakaolin, calcined clays, FA or blast furnace slag by action of an alkali in an aqueous medium [27] [1]. Activation by alkaline compounds (Na,K)OH, $(Na,K)_2CO_3$, Na,K silicates (water glass) gives rise to geopolymeric amorphous materials [28] [29]. During geopolymerization, other phases such as C–S–H phase, crystalline C–A–S–H phase, and possibly zeolites may also be formed [30]. Calcined clays can also be used in the production of lime-pozzolan cements [31], where CaO or $Ca(OH)_2$ is applied to produce standalone cement. Calcined clays can also be used to produce hardened cement with the source of magnesia [32] or with phosphoric acid to produce acid geopolymers [33].

The work presented utilizes the knowledge obtained both from literature and extensive research into FBC ashes. It describes the synthesis of a binder, which, in its composition, is similar to FBC ashes and can be prepared under laboratory conditions [13] [15]. With increasing pressure to reduce coal mining, the knowledge gained from studying FBC ashes may be used to synthesize a sustainable hydraulic binder based on calcined clays, which displays rather interesting properties. Some of its applications aim to replace cement and thus reduce the carbon footprint [34]. Also, our study experimentally confirmed the stability of the binder during the period of 2.8 years.

EXPERIMENTAL

Characterization of raw materials

Three types of basic raw materials were used to prepare different binders. Metakaolin produced under the brand name Mefisto (by Lupkové závody, Nové Strašecí, CZ) was used as a source of aluminosilicates – it is produced from natural clay (stone clay) and calcined in a rotary kiln (labeled Mk). The second type of raw materials were the substances containing sulfur, namely $CaSO_4$ anhydrite II (produced by Anhydritec GmbH, BRD) made from gypsum obtained during flue gas desulfurization and calcined in a rotary kiln, and $CaSO_4 \cdot 2H_2O$ gypsum coming from the Počerady power plant, CZ. The third type of raw material was represented by CaO lime (produced by Limestone Čertovy schody a.s., Lhoist, CZ) obtained from limestone from the location Čertovy schody CZ, which was calcined in the Maerz shaft kiln, or by hydrated lime $Ca(OH)_2$ from the identical production. The raw materials gained from calcination processes were ground in an industrial rotary mill. The elemental composition of the obtained raw materials as determined by X-ray fluorescence (XRF) analysis is presented in Table 1. Loss on ignition (LOI) was determined gravimetrically for samples of Mk, $CaSO_4$ anhydrite II and CaO according to regulation EN 196-2 at 950 °C. However, LOI was not determined for $CaSO_4 \cdot 2H_2O$ and $Ca(OH)_2$ due to their phase transitions. Table 2 shows the composition of crystalline phases in the raw materials measured via X-ray diffraction (XRD) supplemented with other parameters such as specific density, specific surface area and mean particle size D50, respectively quantiles D10 and D90.

Table 1. XRF Analysis of Raw Materials; Metakaolin Mk, $CaSO_4$ Anhydrite II, $CaSO_4 \cdot 2H_2O$, CaO Lime and $Ca(OH)_2$ hydrated lime. *not relevant.

wt. %	Al_2O_3	SiO_2	CaO	MgO	K_2O	Fe_2O_3	TiO_2	SO_3	LOI
Mk	42.49	49.62	0.24	0.25	1.07	2.61	1.15	0.02	2.20
$CaSO_4$ anhydrite II	0.17	0.50	44.48	0.09	0.03	0.15	0.00	54.21	0.30
$CaSO_4 \cdot 2H_2O$	0.78	1.00	46.11	0.40	0.04	0.11	0.02	51.39	*
CaO	0.05	0.11	98.60	0.83	0.02	0.06	0.00	0.14	0.10
$Ca(OH)_2$	0.00	0.02	99.09	0.72	0.01	0.03	0.01	0.05	*

Table 2. XRD phase analysis of raw materials and selected physical properties; specific density; specific surface and quantiles D10, D50 and D90, *traces.

	Mk	$CaSO_4$ anhydrite II	$CaSO_4 \cdot 2H_2O$	CaO	$Ca(OH)_2$
Phase composition majority > 80 %	amorphous phase	anhydrite	gypsum	lime	portlandite
Phase composition minority < 10 %	quartz, kaolinite, mullite, muscovite	*portlandite, *CaO, *Quartz	calcite	portlandite, calcite	calcite
Specific density [$kg \cdot m^{-3}$]	2 429	2 857	2 210	3 052	2 118
Specific surface area [$m^2 \cdot kg^{-1}$]	1 590	362	113	772	1 409
D10	1.09	1.91	5.07	1.31	1.40
D50	3.78	22.71	57.45	12.46	8.49
D90	12.24	59.89	112.30	78.45	66.73

Mixture preparation

Two sets of mixtures were prepared. The first series of mixtures (labeled Mk1 – Mk5) contained metakaolin Mk and variable components with sulfur ($CaSO_4 \cdot 2H_2O$ and $CaSO_4$ anhydrite II) and lime (CaO, $Ca(OH)_2$), as shown in Table 3. The second series consisted of 28 mixtures (labeled as 1-28) prepared with differing ratios of individual components of metakaolin Mk, $CaSO_4$ anhydrite II and lime CaO. The ternary diagram in Figure 1 indicates the area examined in the prepared mixtures. Homogenization of dry components was carried out in a laboratory digital mortar mixer 39-0045 (ELE International) using a low speed program of 62 rpm ± 5 rpm for 15 minutes.

Two pastes designated P2 and P12 were made from the dry mixtures prepared with the following composition of individual components: 68 wt. % Mk, 20 wt. % $CaSO_4$ anhydrite II and 12 wt. % CaO (P2 paste), and 45 wt. % Mk, 30 wt. % $CaSO_4$ anhydrite II and 25 wt. % CaO (P12 paste). Their water to binder ratio was $w = 0.38$ (P2) and $w = 0.37$ (P12), respectively. A polycarboxylate-based plasticizer was added to tap water in the amount of 1.5 % by weight of the binder. In comparison, the mortars were prepared with the added content of silica sand of continuous granulometry in the ratio of 1:1.5 to the binder and with the water to binder ratio $w = 0.43$ (mortars labeled M1-M28). The composition of the mortars is provided in Figure 1. From samples Mk1-Mk5, the mortars were prepared in the same manner as in the case of M1 -M28 mortars, with the water to binder ratio w being 0.48.

Table 3. Composition of mixtures Mk1-Mk5 (in wt. %).

wt. %	Mk	CaO	$Ca(OH)_2$	$CaSO_4 \cdot 2H_2O$	$CaSO_4$ anhydrite II
Mk1	70	30	–	–	–
Mk2	70	–	–	–	30
Mk3	50	–	50	–	–
Mk4	68	–	12	20	–
Mk5	68	12	–	–	20

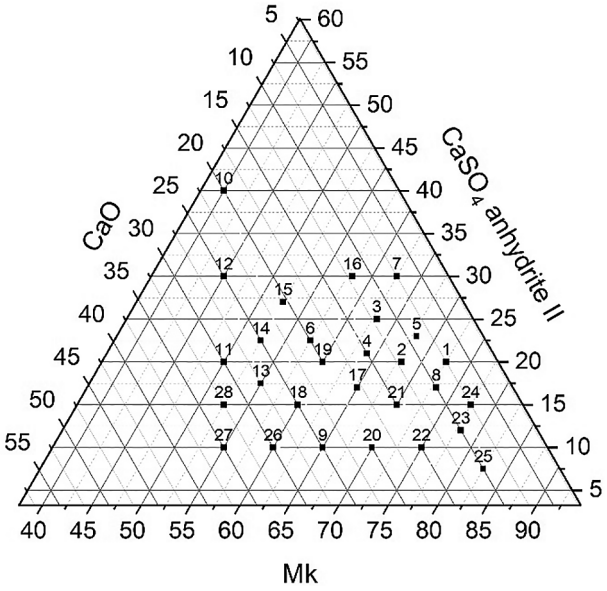

Figure 1. Composition of tested mixtures 1-28 (in wt.%).

From the prepared pastes and mortars, prisms were produced with dimensions of 40 × 40 × 160 mm. The prisms were stored in a curing cabinet in an environment with 95 % relative air humidity. After 24 hours, they were removed from molds and were placed back into the curing cabinet. The prisms formed were stored at the temperature of 20-23 °C, and then subjected to destructive determination of strength within 14 days – – 1 year. The specimens monitored for their length changes in time were prepared and measured according to regulation EN 12617-4 [35]. When removed from molds and after measuring the zero value of their body length, the prisms were placed in two different environments, i.e. stored in the curing cabinet and in the open air. Measurements of changes in length ranged from 1 day to 2.8 years.

Equipment and methods

The elemental composition of the initial raw materials was determined by XRF analysis using a sequential wave dispersion X-ray spectrometer ARL 9400 XP.

The obtained data were evaluated by standardless software Uniquant 4. After destructive strength tests, the samples of the raw materials and pastes were analyzed by X-ray diffraction with the PAN analytical X´Pert PRO instrument and the PDF-4 + 2015 database. An ultrafast PIXCEL detector was employed to collect XRD data over the angular range from 15 to 75° (2θ) with a step size of 0.013° 2θ and a counting time of 180 s/step. Morphology, composition of raw materials and hydrated products were monitored using SEM and EDX analyses with a scanning electron microscope Hitachi S 4700. The hydrated pastes were analyzed by NMR solid state analysis ^{27} Si, ^{21}Al with a Bruker Avance III HD 500 WB/US NMR apparatus.

Analyses of physical properties included examining particle size distribution, specific density (ρ) and specific surface area (S). To determine the particle size distribution, a laser-light scattering analyzer Bettersizer 2600 (Dandong Bettersize Instruments Ltd., China) was employed. Specific density (ρ) was measured by the pycnometric method and the specific surface (S) of the samples was measured by the air permeability Blain method [36].

RESULTS AND DISCUSSION

Lime activation of metakaolin

Lime activation of metakaolin was studied on mortar prisms Mk1-Mk5, as shown in Figure 2. The activation of metakaolin mixtures Mk1 and Mk2 led to problems during solidification. In the case of mixture Mk1, the mixture solidified rather quickly after the addition of CaO, while in the case of mixture Mk2, the addition of $CaSO_4$ anhydrite II resulted in very slow solidification. The reaction of CaO with water is rather swift resulting in an abrupt rise of Ca^{2+} concentration and a quick reaction of CaO with metakaolin [37]. On the other hand, the reaction of $CaSO_4$ anhydrite II with water is quite slow causing a similarly slow reaction of Ca^{2+} ions with metakaolin [38]. In the Mk3 system metakaolin was activated with $Ca(OH)_2$ and for Mk4 activation $CaSO_4{\cdot}2H_2O$ was additionally used. The mixtures achieved measurable strengths ranging from 7 to 42 MPa over a period of 14-90 days. These observations are in accordance with the literature [23-26]. After 90 days, the best strength results of up to 79 MPa were achieved by the mixture of anhydrous components designated as Mk5 (Mk, CaO and $CaSO_4$ anhydrite II), which acted more effectively than the other lime activators tested. The mixture of CaO and $CaSO_4$ anhydrite II has been shown to act synergistically in the process of metakaolin hydration. The reaction heat released during the hydration of CaO is quite likely also involved in the synergistic effect observed [13, 15]. Mortar Mk5 with a binder containing metakaolin Mk, CaO and $CaSO_4$ anhydrite II achieved greater strengths after hardening compared to all the other lime activators, Figure 2.

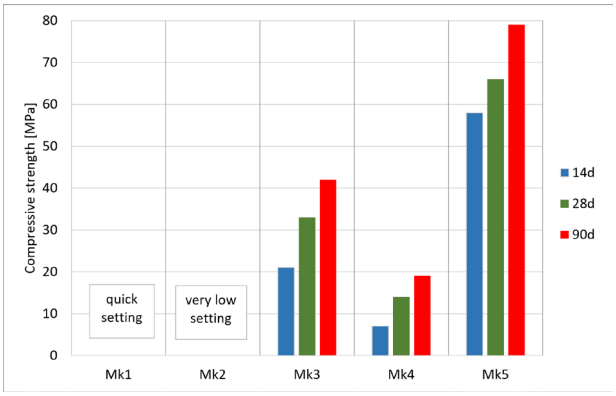

Figure 2. Compressive strength of hardened mortars Mk1-Mk5 after 14-90 days of hydration.

XRD phase analysis

When hydrating the P2 mixture of metakaolin Mk, CaO and $CaSO_4$ anhydrite II, CaO is rapidly hydrated to $Ca(OH)_2$, and ettringite and an amorphous binding phase are formed, as shown in Figure 3. The contents of $Ca(OH)_2$ and $CaSO_4$ anhydrite II decrease gradually, while, in contrast, the content of ettringite rises. Our hydrated binder displayed no crystalline phases of C–A–S–H occurring after the hydration of PC (such as: C_4AH_n, C_3AH_6, C_2ASH_8 gehlenite hydrate, or hydrogranates). After 7 days, a peak appeared at the 10 °2θ position, which may correspond to monosulfate C_4AH_{12}, typically being formed by conversion from ettringite in hydrated PC. CaO, a possible source of expansion phenomena, was not detected in the hardened material.

In the later stages of hydration, ettringite can be modified to yield a solid solution [39]. A good example is the effect of airborne CO_2, which gives rise to single or double substitutions of carbonate replacing sulfate in ettringite, i.e. $Ca_6Al_2[(SO_4)_{1-x}(CO_3)_x]_3(OH)_{12}{\cdot}26H_2O$. Over a longer period of time, ettringite can only be de-

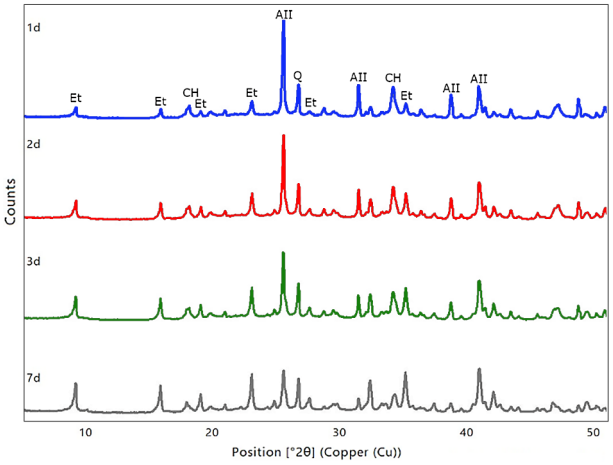

Figure 3. P2 Hardened paste diffractograms after 1, 2, 3 and 7 days of hydration: Ett – ettringite, CH – $Ca(OH)_2$, Q – quartz, AII – $CaSO_4$ anhydrite II.

graded after the formation of minor secondary gypsum $CaSO_4 \cdot 2H_2O$ [40] as shown in Equation 2 and Figure 4.

$$C_6A_3H_{32} + CO_2 \rightarrow 3\ CaCO_3 + \\ + 3CaSO_4 \cdot 2H_2O + Al_2O_3 \cdot nH_2O + \\ + (26 - n)H_2O \quad (2)$$

Ettringite may be further modified by substituting silicon for aluminum to form compounds such as woodfordite $Ca_6Al_2(SO_4,SiO_4,CO_3)_3(OH)_{12} \cdot 26H_2O$, thaumasite $Ca_6(SO_4)_2(CO_3)_2[Si(OH)_6]_2 \cdot 24H_2O$ or cottenheimite $Ca_3Si(OH)_6(SO_4)_2(H_2O)_{12}$ [41].

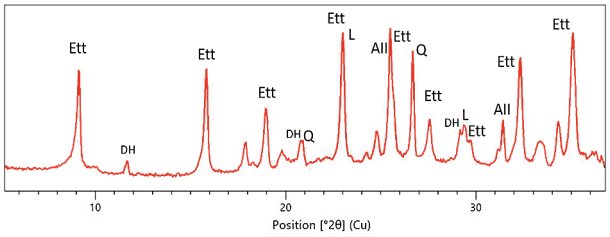

Figure 4. Diffractogram of hardened P2 binder after 2 years of hydration: Ett – ettringite/modified ettringite, Q – quartz, DH – $CaSO_4 \cdot 2H_2O$, L – $CaCO_3$.

SEM analysis

The images of hardened paste P2 show that, after 24 hours of hydration, the residues of metakaolin Mk and $Ca(OH)_2$ can still be detected in the sample, which in the presence of airborne CO_2 changes into calcite $CaCO_3$, as shown in Figure 5a. The amorphous binder phase in which ettringite is dispersed constitutes a major component of the paste, as can be seen in Figure 5b,d. EXD analyses of the binder phase showed that, in addition to calcium and silicon, it also contained aluminum. These observations are consistent with the work of Škvára et al., where, besides the C–S–H phase, the C–A–S–H phase was also detected in the hardened binder of sulfocalcic fly ash [15]. Figure 5c demonstrates an undulating habitus of ettringite crystals, being affected by the addition of a plasticizer.

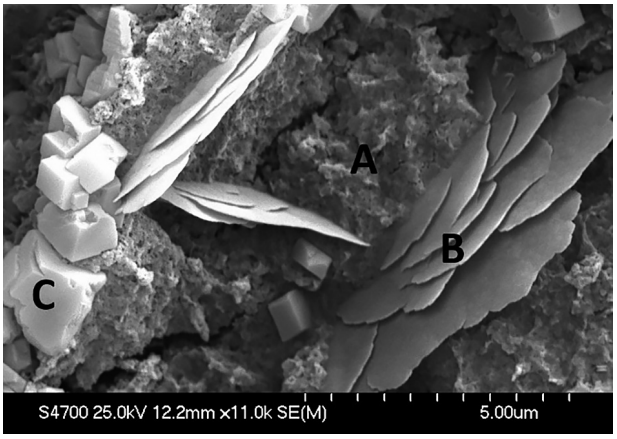

a) 24 h

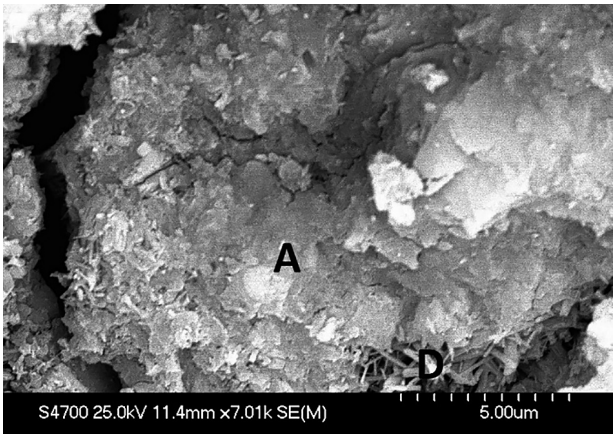

b) 5 d

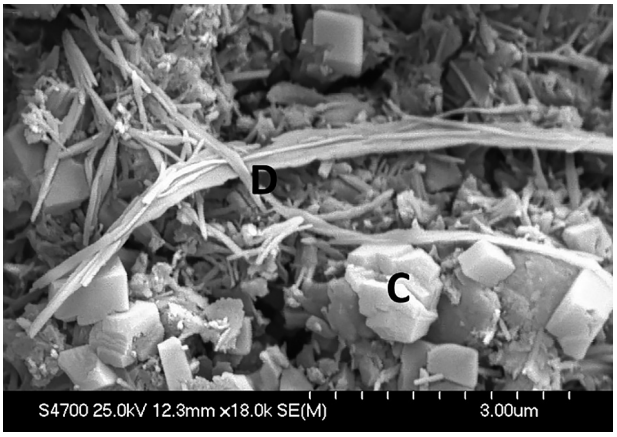

c) 28 d

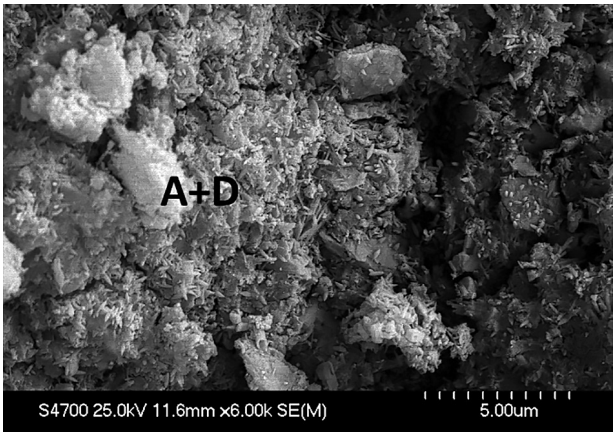

d) 28 d

Figure 5. P2 Hardened paste fracture area after 24 hours (a), after 5 days (b) and after 28 days (c, d) of hydration. A – binder phase, B – unreacted metakaolin, C – calcite, D – ettringite, magnified by 6 000× – 18 000×.

NMR analysis

Concerning the amorphous binder phase in the hydrated sample, NMR ^{21}Al shows that Al is present in the tetrahedral coordination of Al^{IV}, which belongs to the C–A–S–H phase, and also in the octahedral coordination of Al^{VI} belonging to ettringite, as shown in Figure 6. The presence of Al in pentaedric coordination is rather questionable. The same result was shown in the hydrated sulfocalcic fly ash – FA – $Ca(OH)_2$ binder [15]. Al^{IV} coordination was identified in the samples of the binding component of Roman concrete from Baianus Sinus, Portus Neronis and Portus Cosanus [42] [43]however, in first century CE emphasized rock-like cementitious processes involving volcanic ash (pulvis. NMR analyses of hydrated LC^3 cement (calcined clay, limestone and PC) also revealed the presence of Al^{IV} [9]. Coordinations of Q^4(0Al), Q^3 (1Al) and Q^2(1Al) were found in the NMR ^{27}Si spectrum in the amorphous phase of the hydrated binder, as shown in Figure 6. The results indicate the presence of linked SiO_4^{4-} and AlO_4^{5-} tetraedra.

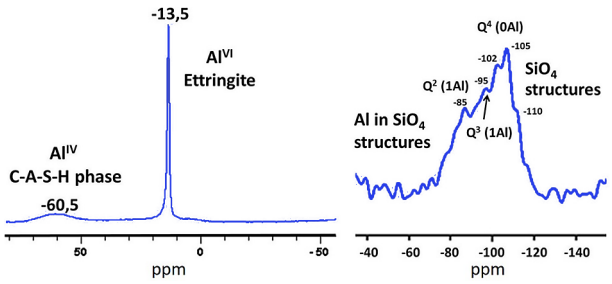

Figure 6. NMR spectra 27Si and 21Al of paste sample P2, 1 year of hydration. AlIV (C–A–S–H phase) /AlVI (ettringite).

Compressive strength of hardened mortars

The research work examined 28 variations of the binder composition of metakaolin Mk, CaO and $CaSO_4$ anhydrite II with the designation M28 focusing on the properties of hardened mortars. After determining compressive strength after 28 days and 1 year, the strength isochars in the ternary diagram were created using the OriginPro 2019 program, as shown in Figure 7. As can be deduced from this Figure, in terms of strength, the optimal composition lies in the vicinity of the composition of mixtures M2, M4, M17 and M21, i.e. 68-70 % Mk, 15-20 % $CaSO_4$ anhydrite II, 12-18 % CaO. The mortars with the optimal composition reached strengths above 85 MPa after 1 year of storage under humid conditions. When a CaO content dropped below 10 % and a $CaSO_4$ anhydrite II content exceeded 30 %, the strengths of the mortars decreased significantly.

Long-term stability

Long-term volumetric stability was demonstrated in hardened composite binder M2 prepared from meta-

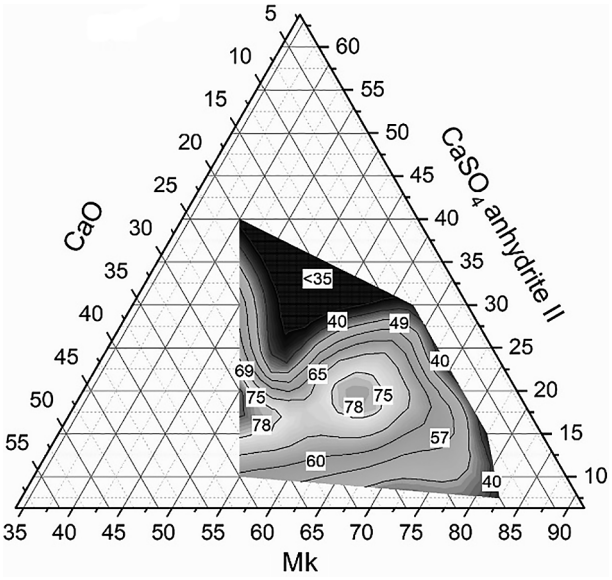

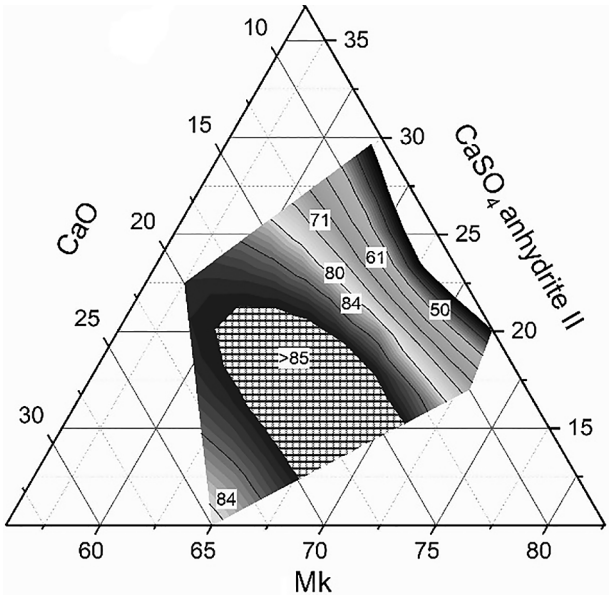

Figure 7. M1-M28 mortar compressive strengths after 28 days (a) and 1 year (b) of hydration, MPa lines in metakaolin system Mk–CaO–$CaSO_4$ anhydrite II (wt. %).

kaolin Mk, CaO, $CaSO_4$ anhydrite II and sand and subsequently observed for a period of 2.8-years when the composite prisms tested were stored under wet and air conditions, as shown in Figure 8.

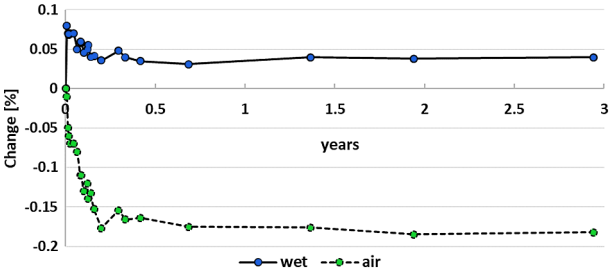

Figure 8. Linear length change measurements of hardened M2 mortar prisms. The samples were stored under laboratory conditions (air) and in the curing cabinet (RH 95 %).

With respect to their long-term behavior over a wide range of compositions, hardened mixtures of metakaolin Mk, CaO and $CaSO_4$ anhydrite II were shown to be stable in volume. However, if the contents of $CaSO_4$ anhydrite II and CaO exceeded 40 %, the test specimens visibly expanded until they got destroyed. Figure 9 shows an approximate boundary for the formation of visible expansion in the metakaolinite system of Mk, $CaSO_4$ anhydrite II and CaO after 14 days.

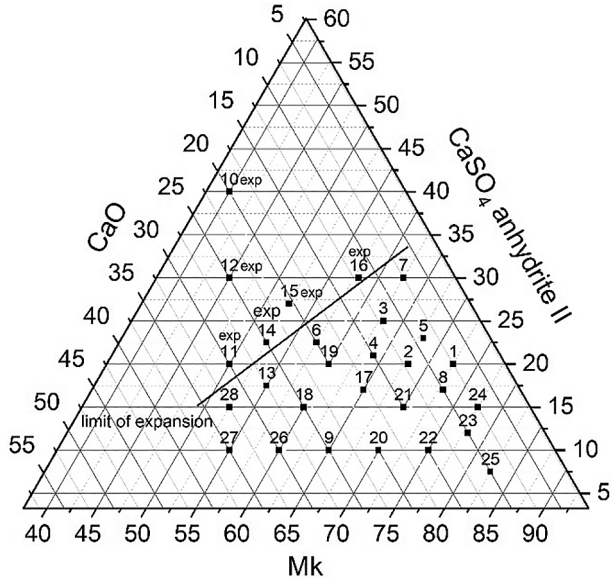

Figure 9. Regions of forming expansion reactions in hydrated mixture of metakaolin Mk, CaO and $CaSO_4$ anhydrite II (component ratios in wt. %), M1-M28, 14 days of hydration.

Figure 10 provides an SEM image showing the fracture surface of the expanding section in sample P12 after 14 days of hydration. The composition of the fibrous expanding part indicates the presence of Ca, S, Al and Si (EDX analysis). In addition to ettringite, modified ettringite is present in hydrated hardened binder P12, where a portion of Al ions is replaced by ions of Si. Therefore, it can be assumed that when high contents of CaO and $CaSO_4$ anhydrite II are present, it is not just the Al component in aluminosilicates (formation of ettringite) that participates in the initial hydration reactions leading to sulfate hydrates, but also part of Si ions play a role here (formation of modified ettringite, kottenheimite).

CONCLUSIONS

Our research has shown that it is possible to produce a hydraulic binder synthetically from metakaolin, anhydrous CaO and $CaSO_4$ anhydrite II, and the binder prepared manifests long-term stability. Also, the novel binder displays properties comparable to those of PC, but it can be produced under significantly lower temperature of 850 °C. Its composition and properties are rather similar to the binders based on FBC ash. At the same time, the material mixture of the new binder may be modified just as readily as PC. The hydrated binder consisting of metakaolin Mk, $CaSO_4$ anhydrite II and CaO has a different product composition than hydrated PC. Its binding phase is formed by an amorphous C–A–S–H phase and a C–S–H phase. The presence of the C–A–S–H phase indicates a similarity to Roman cement. Crystalline hydration products are present in the binder - namely ettringite or modified ettringite, and, to a limited extent, also $CaCO_3$, $Ca(OH)_2$, and $CaSO_4 \cdot 2H_2O$. No crystalline phases from the C–A–S–H system and zeolites were detected. The binder achieves strengths that are comparable to those of PC. The binder was found to be stable in its volume in the long-term period of 2.8 years. When the contents of CaO and $CaSO_4$ anhydrite II in the mixture with metakaolin exceeded 40 %, expansion phenomena were observed leading to the destruction of the test prisms.

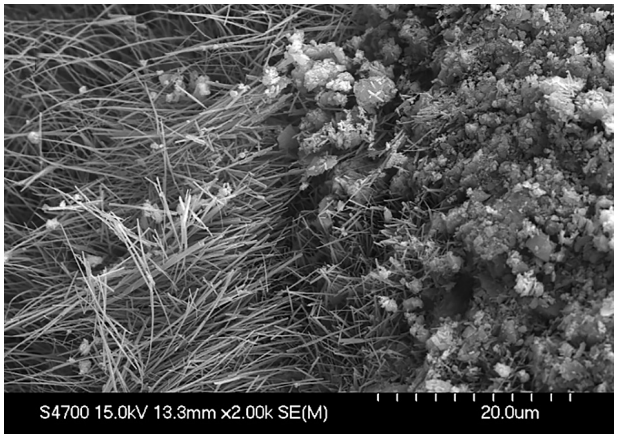

a) 2000×

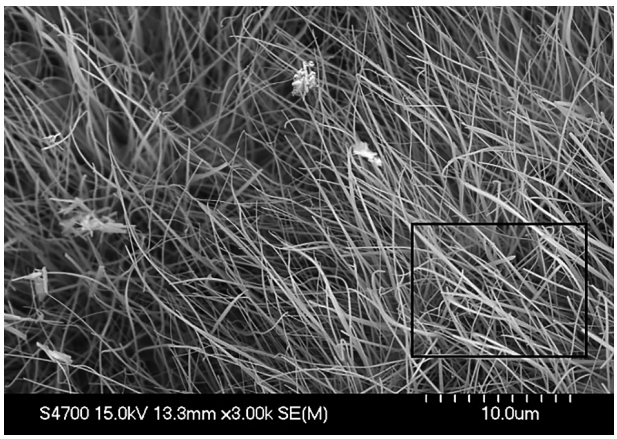

b) 3000×

Figure 10. Fracture area of expanding section in sample P12 with marked region analysed, 14 days of hydration, magnification 2000× (a) and 3000× (b).

Acknowledgements

This project was co-financed with the state support of the Technology Agency of the Czech Republic within the scope of TREND Program FW01010195.

REFERENCES

1. Hanein T., Thienel K.C., Zunino F., Marsh A.T.M., Maier M., Wang B., Canut M., Juenger M.C.G., Ben Haha M., Avet F., et al. (2022): Clay calcination technology: state-of-the-art review by the RILEM TC 282-CCL. *Materials and Structures, 55*, 3. doi: 10.1617/s11527-021-01807-6
2. Fernandez R., Martirena F., Scrivener K. L. (2011): The origin of the pozzolanic activity of calcined clay minerals: A comparison between kaolinite, illite and montmorillonite. *Cement and Concrete Research*, *41*(1), 113-122. doi: 10.1016/j.cemconres.2010.09.013
3. Scrivener K., Favier A. (2015). *Calcined clays for sustainable concrete*. RILEM.
4. Martirena F., Favier A., Scrivener K. (2018). Calcined Clays for Sustainable Concrete. *RILEM Bookseries.* doi: 10.1007/978-94-024-1207-9
5. Bishnoi S. (2020): Calcined Clays for Sustainable Concrete. In: *Proceedings of the 3rd International Conference on Calcined Clays for Sustainable Concrete*, Springer, Singapore.
6. Justnes H., Østnor T.A. (2015): Alternative binders based on lime and calcined clay. *RILEM Bookseries*, *10*, 51–57.
7. Ermilova E. U., Rakhimov R. Z., Kamalova Z. A., Bulanov P. E. (2018): Calcined mixture of clay and limestone as a complex additive for blended Portland cement. *ZKG INTERNATIONAL*, *71*(11), 58-67.
8. Steenberg M., Herfort D., Poulsen S.L., Skibsted J., Damtoft J.S. (2011). Composite cement based on Portland cement clinker, limestone and calcined clay. In: P*roceedings of the XIII International Congress on the Chemistry of Cement*, p. 97.
9. Scrivener K., Martirena F., Bishnoi S., Maity S. (2018): Calcined clay limestone cements (LC3). *Cement and Concrete Research*, *114*, 49-56. doi: 10.1016/j.cemconres.2017.08.017
10. Ohenoja K., Pesonen J., Yliniemi J., Illikainen M. (2020): Utilization of fly ashes from fluidized bed combustion: A review. *Sustainability*, *12*(7), 2988. doi: 10.3390/su12072988
11. Anthony E. J., Granatstein D. L. (2001): Sulfation phenomena in fluidized bed combustion systems. *Progress in energy and Combustion Science*, *27*(2), 215-236. doi: 10.1016/S0360-1285(00)00021-6
12. Gazdič D., Fridrichová M., Kulísek K., Vehovská L. (2017): The potential use of the FBC ash for the preparation of blended cements. *Procedia Engineering*, *180*, 1298-1305. doi: 10.1016/j.proeng.2017.04.292
13. Škvára F., Šulc R., Snop R., Cílová Z.Z., Peterová A., Kopecký L., Formácek P. (2016): Czech fluid Sulfocalcic ash and fly ash. *Ceramics – Silikáty*, *60*, 344–352. doi: 10.13168/cs.2016.0051
14. Robl T., Oberlink A., Jones R. (2017). *Coal Combustion Products (CCPs): Characteristics, Utilization and Beneficiation*; 1st ed.; Woodhead publishing, ISBN 9780081010471.
15. Škvára F., Šulc R., Snop R., Peterová A., Šídlová M. (2018): Hydraulic clinkerless binder on the fluid sulfocalcic fly ash basis. *Cement and Concrete Composites*, *93*, 118-126. doi: 10.1016/j.cemconcomp.2018.06.020
16. Lothenbach B., Scrivener K., Hooton R. D. (2011): Supplementary cementitious materials. *Cement and Concrete Research*, *41*(12), 1244-1256. doi: 10.1016/j.cemconres.2010.12.001
17. Pollio M.V. (2010). *De architectura libri decem*; TeMi, ISBN 978-80-86410-58-6.
18. Brandon C., Hohlfelder R.L., Jackson M.D., Oleson J.P. (2014). *Bulding for eternity: The History and Technology of Roman Concrete Engineering in the Sea*; Oxbow Books.
19. Rivera-Villarreal R., Cabrera J.G. (1999). Microstructure of Two-Thousand-Year Old Lightweight Concrete. In: *Proceedings of the International Concrete Research – Special Publication, 186*; 183–200.
20. O'Kon J.A. (2012). *The lost secrets of Maya technology*; New Page Books,ISBN 160163207X.
21. Villaseñor Alonso I. (2010). Building Materials of the Ancient Maya: A Study of Archaeological Plasters.
22. Shi C., Roy D., Krivenko P. (2003). *Alkali-activated cements and concretes*. CRC press.
23. Žemlička M., Kuzielová E., Kulieffayová M.; Tkacz J., Palou M.T. (2015): Study of hydration products in the model systems metakaolin-lime and metakaolin-lime-gypsum. *Ceramics - Silikáty, 50*, 283–291.
24. Majerova J., Drochytka R. (2018). The influence of the addition of gypsum on some selected properties of lime-metakaolin mortars. In: *IOP Conference Series: Materials Science and Engineering* (Vol. 385, No. 1, p. 012034). IOP Publishing. doi: 10.1088/1757-899X/385/1/012034
25. Taha A. S., Serry M. A., El-Didamony, H. (1985): Hydration characteristics of metakaolin–lime–gypsum. *Thermochimica acta*, *90*, 287-296. doi: 10.1016/0040-6031(85)87106-9
26. Morsy M. S., Al-Salloum Y. A., Almusallam T. H., Abbas H. (2017): Mechanical properties, phase composition and microstructure of activated Metakaolin-slaked lime binder. *KSCE Journal of Civil Engineering*, *21*(3), 863-871. doi: 10.1007/s12205-016-0667-2
27. Rashad A. M. (2013): Alkali-activated metakaolin: A short guide for civil Engineer – An overview. *Construction and Building Materials*, *41*, 751-765. doi: 10.1016/j.conbuildmat.2012.12.030.
28. Davidovits J. (2020). *Geopolymer chemistry and applications*; Institut Géopolymère, ISBN 9782954453118.
29. Alonso S., Palomo A. (2001): Alkaline activation of metakaolin and calcium hydroxide mixtures: influence of temperature, activator concentration and solids ratio. *Materials Letters*, *47*(1-2), 55-62. doi: 10.1016/S0167-577X(00)00212-3
30. Duxson P., Fernández-Jiménez A., Provis J. L., Lukey G. C., Palomo A., van Deventer J. S. (2007): Geopolymer technology: the current state of the art. *Journal of Materials Science*, *42*(9), 2917-2933. doi: 10.1007/s10853-006-0637-z
31. Boonjaeng S., Chindaprasirt P., Pimraksa K. (2014): Lime-calcined clay materials with alkaline activation: phase development and reaction transition zone. *Applied clay science*, *95*, 357-364. doi: 10.1016/j.clay.2014.05.002
32. Ruan S., Liang S., Kastiukas G., Zhu W., Zhou X. (2020): Solidification of waste excavation clay using reactive magnesia, quicklime, sodium carbonate and early-age oven

curing. *Construction and Building Materials*, *258*, 120333. doi: 10.1016/j.conbuildmat.2020.120333

33. Gualtieri M. L., Romagnoli M., Pollastri S., Gualtieri A. F. (2015): Inorganic polymers from laterite using activation with phosphoric acid and alkaline sodium silicate solution: mechanical and microstructural properties. *Cement and Concrete Research*, *67*, 259-270. doi: 10.1016/j.cemconres.2014.08.010
34. Šmilauer V., Sovják R., Pešková Š., Šulc R., Škvára F., Šídlová M., et al. (2021): Shotcrete using ternary binder made from coal combustion products: from lab tests to an application. *IOP Conference Series: Materials Science and Engineering*, *1205*, 012004. doi: 10.1088/1757-899x/1205/1/012004
35. EN 12617-4 (2003). Products and systems for the protection and repair of concrete structures – Test methods – Part 4: Determination of shrinkage and expansion, European Committee for Standardization.
36. EN 196-6 (2019). Methods of testing cement – Part 6: Determination of fineness, European Committee for Standardization.
37. Oates J. A. (2008). *Lime and limestone: chemistry and technology, production and uses*. John Wiley & Sons.
38. Singh N. B. (2005): The activation effect of K_2SO_4 on the hydration of gypsum anhydrite, $CaSO_4$ (II). *Journal of the American Ceramic Society*, *88*(1), 196-201.doi:10.1111/j.1551-2916.2004.00020.x
39. Glasser F.P. (2022). The stability of ettringite. In: *Proceedings of the International RILEM TC 186-ISA Workshop on Internal Sulfate Attack and Delayed Ettringite Formation*, Vol. 5, pp. 43–63.
40. Nishikawa T., Suzuki K., Ito S., Sato K., Takebe T. (1992): Decomposition of synthesized ettringite by carbonation. *Cement and Concrete Research*, *22*(1), 6-14. doi: 10.1016/0008-8846(92)90130-N
41. Chukanov N. V., Britvin S. N., Van K. V., Möckel S., Zadov A. E. (2012): Kottenheimite, $Ca_3Si(OH)_6(SO_4)_2 \cdot 12H_2O$, a new member of the ettringite group from the Eifel area, Germany. *The Canadian Mineralogist*, *50*(1), 55-63. doi: 10.3749/canmin.50.1.55.
42. Jackson M. D., Chae S. R., Mulcahy S. R., Meral C., Taylor R., Li P.,et al. (2013): Unlocking the secrets of Al-tobermorite in Roman seawater concrete. *American Mineralogist*, *98*(10), 1669-1687. doi: 10.2138/am.2013.4484.
43. Jackson M. D., Mulcahy S. R., Chen H., Li Y., Li Q., Cappelletti P., Wenk H. R. (2017): Phillipsite and Al-tobermorite mineral cements produced through low-temperature water-rock reactions in Roman marine concrete. *American Mineralogist*, *102*(7), 1435-1450. doi: 10.2138/am-2017-5993CCBY